Zeitschrift für Physikalische Chemie, Bd. 197, S. 67–96 (1996)

The Reaction of Molecular Oxygen with Silver at Technical Catalytic Conditions: Bulk Structural Consequences of a Gas-Solid Interface Reaction

By D. Herein, A. Nagy, H. Schubert, G. Weinberg, E. Kitzelmann and R. Schlögl

Fritz-Haber-Institut der Max-Planck-Gesellschaft, Faradayweg 4–6, D-14195 Berlin, FAX-30/8413-4401

Dedicated to Gerhard Ertl on the occasion of his 60th birthday

(Received May 24, 1996)

X-ray diffraction / Thermal desorption spectroscopy / Methanol oxidation / Catalysis

Powder X-ray diffraction (XRD), microscopic examinations and temperature-programmed desorption (TDS) of molecular oxygen from polycrystalline silver foils and granules were used to study its interaction with oxygen in a pressure range between 0.01 mbar and 300 mbar and in a temperature interval between 525 K and 1000 K.

Massive re-structuring in (110) oriented crystallites and the transformation of textured foils into single-crystalline-like ordered materials were found in ambient air oxidation. High resolution XRD lineprofile analysis led to the detection of a symmetry lowering of the initially fcc cubic silver lattice to an orthorhombic distorted form (a = 409.2 pm, b = 289.6 pm, c = 288.6 pm) with a slight deviation of the atomic co-ordinates of the silver creating channels perpendicular to the (110) direction through which oxygen may diffuse into the bulk. At 300 mbar oxygen partial pressure the re-structuring transforms into a preferential orientation in the (331) direction with an even better ordering of the crystallites than observed in air oxidation. The TDS results confirmed the existence of three atomic oxygen species located at the surface, (T_{des} 575 K) in the interface (T_{des} 900 K) and as bulk-dissolved species (T_{des} 700 K). Pre-saturation of the samples allowed to obtain consistent isothermal TDS data sets from which the unperturbed desorption features of all three species were extracted. The role of the bulk-dissolved species in controlling the intermixing of the three species is discussed.

The performance of silver in the partial oxidation of methanol is directly related to the individual desorption features of the three oxygen species. It was confirmed that the strongly held interface species plays an important role in the overall conversion perfor-

mance of the catalyst. The bulk-dissolved species provides a significant abundance of the surface atomic species also required in catalysis which would be fully desorbed at reaction temperature, if only the gas-interface adsorption channel would exist for its population.

Die Reaktion von polykristallinem Silbermetall mit molekularem Sauerstoff wurde im Druckbereich 0.01 mbar bis 300 mbar und bei Temperaturen von 525 K bis 1000 K untersucht. Dazu wurden Röntgenbeugung an Pulvern (XRD), thermische Desorption (TDS) und mikroskopische Methoden eingesetzt. Proben waren Bleche und elektrolytisch hergestelltes Silbergranulat.

Bei Reaktionen in synthetischer Luft wurden erhebliche strukturelle Modifikationen festgestellt, die zum einen eine Texturierung der Proben bis zur Qualität von Einkristallen in die (110) Richtung umfaßte. Genaue Strukturbestimmungen führen zur Detektion einer Symmetrieerniedrigung der Atomanordnung von kubisch nach orthorhombisch (a = 409.2 pm, b = 289.6 pm, c = 288.6 pm), die in (110) Richtung eine kanalartige Verzerrung schafft, welche die Volumendiffusion von Sauerstoff erleichtert. Bei Erhöhung des Partialdruckes wandelt sich die Texturierung in die (311) Richtung um.

Die TDS Resultate bestätigen literaturbekannte Daten und weisen drei, in ihrer Konzentration voneinander abhängige Formen von atomarem Sauerstoff in Silber mit Desorptionstemperaturen von 575 K, 700 K und 900 K nach. Durch Vorsättigung des Volumens mit Sauerstoff wurde die Auflösung der TDS-Daten soweit verbessert, daß die drei Desorptionprozesse einzeln isoliert werden konnten. Die Analyse dieser Daten zeigte, daß alle drei Formen benötigt werden, um die Wirkung von Silber als Selektivkatalysator in der Partialoxidation von Methanol zu Formaldehyd zu erklären. Die Bedeutung der drei Formen von Sauerstoff für die Epoxidation von Ethylen wird diskutiert.

Introduction

The reaction between silver metal and molecular oxygen is a key elementary step in the catalytic application of silver for selective oxidation reactions [1]. The industrial significance of ethylene epoxidation and methanol to formaldehyde conversion has triggered much scientific interest [2]. Methanol oxidation as technical process is carried out [3] over unsupported silver with no addition of promoter species. This situation is ideally suited to the application of the "single crystal approach" strategy to analyse a chemical reaction. Nevertheless, significant uncertainties still exist over the abundance and exact chemical nature of the various oxygen species identified so far in the process [1, 2, 4].

The chemistry of the silver-oxygen interaction is special compared to the reaction of most other metals with oxygen, as the most stable reaction product, an oxide, does not exist for silver at elevated temperatures and atmospheric pressure [5]. In most other cases the interaction of oxygen with metals leads via various adsorbate phases and surface re-structuring processes to sub-surface compounds and to oxides forming either parallel to, or as consequence of, the sub-surface compounds. Fig. 1 reveals the standard heat of formation of oxides from the elements for silver and its neighbour in the periodic table, for copper. Copper is a metal with stable oxide phases existing over the whole temperature range of catalytic interest at an oxygen activity resulting from atmospheric pressure of dioxygen. This

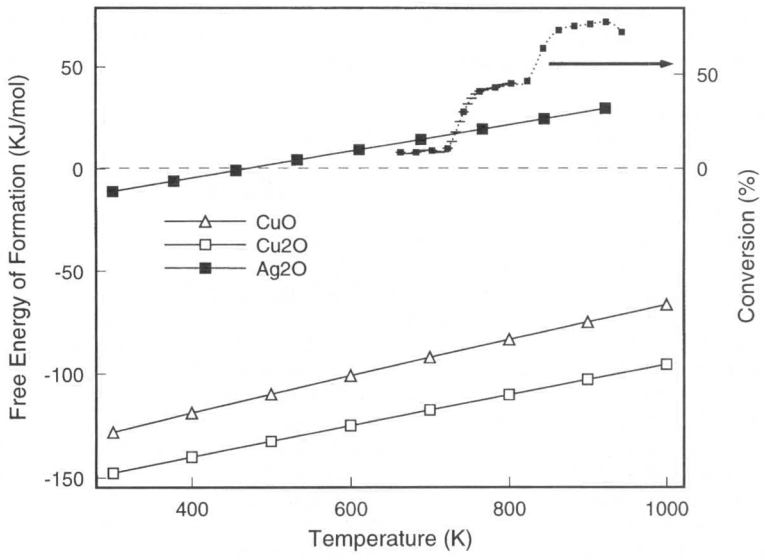

Fig. 1. Free energy of formation of binary oxides from the elements at standard conditions. For comparison, a section through a conversion vs. temperature diagram for the methanol to formaldehyde reaction (1:1 water, methanol, methanol to oxygen ratio 125:100, SV 100.000) over granular silver (sample 4) is included.

is not the case for silver, where the most stable oxide Ag_2O exhibits a positive free energy of formation above 450 K. Thermodynamics show that at catalytic conditions, there exists only a bi-phasic situation. Nevertheless, it was speculated on the basis of electrochemical experiments that a special oxide could play an important role in catalysis [6]. Fig. 1 shows that this is not to be expected for the reaction of methanol to formaldehyde which exhibits significant conversion only at temperatures where no silver oxide should exist. *In-situ* X-ray diffraction may be used to check the possibility that a transient oxide species might exist under reaction conditions. In consideration of the thermodynamic instability of the methanol molecule in oxygen at 900 K, where the technical reaction is operated, it is to be expected that only a non-oxidic surface will act as a catalyst for partial oxidation to formaldehyde, as an oxide would be reduced to the metal under total oxidation of methanol to carbon dioxide.

The methanol reaction produces under technical conditions a significant amount of molecular hydrogen besides the expected by-product water [3, 7]. This has led to the assumption that two independent reaction pathways, namely dehydrogenation and oxi-dehydrogenation should be operative in this reaction [7–9]. Two different types of active centres are required for this reaction, none of which should be a binary oxide phase. Indeed, a

Table 1. Literature observations of various oxygen species adsorbed on silver surfaces. The conditions of substrate structure, dosing and detection are different in the sources quoted. The temperature refers to desorption peaks.

Species	Temperature (K)	Localization	Designation	Reference
O_2	25	surface	physisorbed	18
O_2	190–300	surface	chemisorbed	1,4,6,7,13,23
O	595±25	surface	atomic adsorbed	5,13,14,23–26
O	1120	sub-surface	strongly bound	27
O	820	near defects	species V	3,5,9
O	830±50	bulk-dissolved	–	1,5,14,26
O	580	surface	ionic	28
O	800±60	surface-embedded	covalent	28, 29
O	900	–	very high T	14
O	619	sub-surface	–	13
O	580	surface	β	23
O	≤600	surface	α	4,8,10
O	600–900	bulk-dissolved	β	4,8,10
O	≤900	surface-embedded	γ	8,10

number of different states of adsorbed oxygen present on and underneath the surface of metallic silver have been described in the literature. These species have been termed in different notations with partly conflicting designations. Table 1 reports an incomplete list of literature obervations with designations, locations and desorption temperatures as characteristic observables. There is now general agreement that three different species exist which have been located at, in and under the silver surface. Besides TDS, various other spectroscopic techniques have been used [10, 11] to verify the location of these differently designated species. It is noted that in our first publication [12] the assignment of the three oxygen species was incorrect, which was, however, rectified in reference [4] and in all subsequent papers.

It is purpose of the present work to investigate the existence of the several oxygen chemisorption species under sorption conditions relevant for the technical methanol oxidation process [8, 13, 14]. It will become apparent that under such conditions the surface of the silver undergoes re-structuring processes which affect not only the surface structure [14–16] but which are clearly detectable by bulk-sensitive techniques [17] such as powder XRD. The catalyst modifies its whole structure under the combined influence of high temperature and high partial pressures of oxygen. The relationship between chemisorption and bulk structural transformation will be investigated. The results will be used to briefly discuss the extent to which the "single crystal approach" can be literally used to investigate a heterogeneous catalytic reaction under technical conditions.

Experimental

Sample treatment

X-ray diffraction experiments were done with pristine Ag-foil (Aldrich, impurities less then 0.01%, thickness: 0.5 mm). Temperature-programmed oxidation experiments were carried out in addition to foil samples also on silver particles supplied by Aldrich and Goodfellows. The gases used for oxidation of the Ag-foil were of 5.0 quality (Linde). The following samples were prepared for the experiments described here.

Sample 1: Untreated Ag-foil as received from Aldrich.

Sample 2: Ag-foil heated for 24 h at 1073 K in a stream of 20% oxygen in argon.

Sample 3: Ag-foil heated for 24 h at 1073 K in a stream of pure oxygen.

Sample 4: Silver grains of 30 and 60 mesh diameter. These irregular shaped particles served as model material for industrial electrolytic silver catalysts.

Sample 5: Silver grains after pre-treatment in molecular oxygen at 873 K for 58 h (in a quartz tube at 30 ml/min)

The silver foils were pre-treated in 0.1 molar nitric acid for 24 h, washed with triply distilled water and dried in air in order to remove for the TDS analysis possible residual contaminations from the foil manufacturing process. The silver granules were used as received.

X-ray diffraction

The X-ray powder diffraction patterns were recorded in Bragg-Brentano geometry using a rotating sample holder on a STOE STADI P diffractometer equipped with a secondary monochromator (Cu K_α radiation) and a scintillation detector. A step width of 0.04°2Θ was used for the 2Θ-scans. The Ω-scans (rocking curves) were recorded using a step width of 0.02°Ω.

The whole orientational distribution of the micro-crystallites (texture analysis) inside the Ag-foil was determined by Θ/Ω-scans with coupled 2Θ-/Ω-circles (step with ratio 2Θ/Ω = 2:1). The relative orientation of the silver micro-crystallites was determined by Ω-scans at the (111)-reflection of silver. The scintillation detector position (2Θ-circle) was fixed at the maximum counting rate of the $K_{\alpha 1}$-part of the (111)-reflection of each sample. The exact position was determined by profile analysis of the reflection in the corresponding diffraction pattern. The diffraction conditions and the diffraction geometry for Ω-scans are schematically shown in Fig. 2.

Temperature-programmed desorption

The TDS experiments were carried out in two instruments equipped with quartz reactors and external heaters. The heating rate was fixed to 1K/s after variable heating rate experiments revealed this rate to be the best

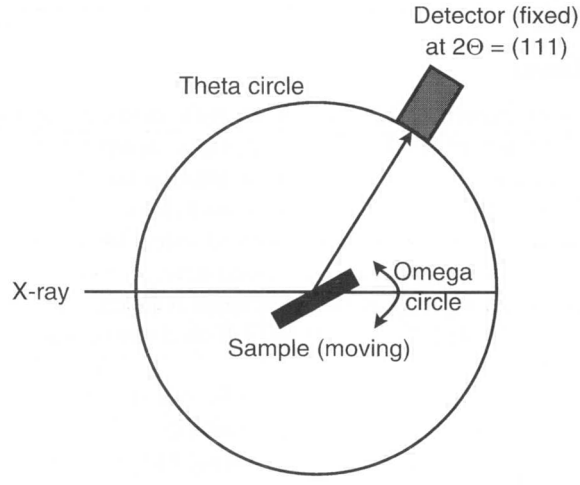

Fig. 2. Diffraction conditions for omega-scans (rocking curve) in Bragg-Brentano geometry in real space. The detector position was fixed at Bragg conditions for the (111)-reflection of silver.

compromise between sensitivity and resolution which is lost in fast heating rate experiments due to massive interference from sub-surface diffusion. At heating rates above 10 K/s the features from the bulk-dissolved species disappear in the background of the TDS data (see for example reference [13]).

Both systems were equipped with facilities allowing to dose purified oxygen (6.0, molecular sieve trap) at pressures between 0.01 mbar and 300 mbar. Mass spectrometers (Balzers QMG 112 and Hiden HAL) interfaced to suitable data aquisition and manipulation systems were used for detection. The temperature deviation of the metal sample relative to the outer wall of the quartz reactor (as large as 70 K) was calibrated for all heating rates and absolute temperatures and is corrected in all data shown. The instruments differed in their vacuum design giving rise to different pumping speeds and detection sensitivities. A significant qualitative difference in the resulting data was not detectable taking the desorption traces from two different silver foils under the same treatment conditions as reference.

All experiments were done with fixed time intervals for cooling in oxygen, pumping down and after-ramp cooling so that potential effects of contamination and structural relaxation should have the same effect on all data.

Samples of 1.0 cm^2 foil and 1492 mg granules were used for the experiments. It is noted that the shape of the TDS profiles was found to depend

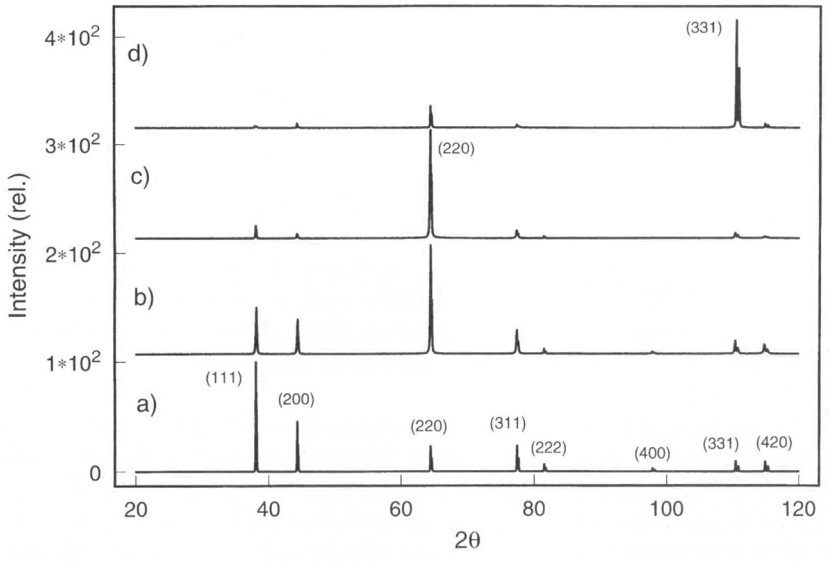

Fig. 3. X-ray powder diffraction patterns of (b) untreated Ag-foil (Sample 1), (c) oxidized Ag-foil in 20% oxygen (Sample 2) and oxidized Ag-foil in 100% oxygen (Sample 3) compared with a calculated diffraction pattern of statistically oriented silver powder (a).

critically on the amount of sample used. Temperature gradients and pumping speed effects seem to affect the data although the surface area of the materials was always purely geometric and below 0.5 m^2/g (Kr-BET data).

Results

X-ray diffraction

The X-ray diffraction experiments were only useful with the silver foil (samples 1−3) as the grains cause by their coarse nature severe complications in the diffracted beam line profile analysis.

Fig. 3 summarizes wide scan data of the three foil samples together with a calculated diffraction pattern with the line profile and intensity parameters typical for the present instrument. All samples exhibit only the phase of elemental silver without significant differences in lineshapes indicating the expected "inertness" (see Fig. 1) of silver against oxygen treatment at elevated temperatures. Quite significant changes occurred, however, in the intensity distributions which excludes the notion that silver may be "unreactive" in oxygen. The as-received sample 1 (trace b) shows preferred orientation of the crystallites in the (110) direction relative to the foil surface caused by the plastic deformations during the preparation of the foil. Refer-

ence experiments which are not shown here indicate that under vacuum, nitrogen, Ar and hydrogen this texture does not change up to temperatures of 923 K which is in agreement with literature observations [17]. Prolonged annealing above 3 h is not possible in these atmospheres as silver evaporation destroys the sample. This evaporation is fully suppressed in oxygen atmosphere or in air for reasons discussed already in the literature [15, 17]. Treatment in air (sample 2, trace c in Fig. 3) increases the degree of preferred orientation in the (110) direction which indicates that a specific interaction of oxygen leads not to an oxide formation but to a re-crystallisation of the silver. It is interesting to note that the bulk-re-orientation preferes the same direction which was found in surface science studies to adsorb molecular and atomic oxygen in good geometric feit between substrate and adsorbate [18].

The increase of the oxygen partial pressure from 200 mbar to 1000 mbar (sample 3, trace d in Fig. 3) causes a complete reversal in the preferred orientation which changed from (110) into the (331) direction. This re-orientation together with the much improved orientational ordering (see e.g. the change in intensity of the (111) reflection) points to a qualitatively different interaction of oxygen at high chemical potential with the silver surface inducing a restructuring of the bulk material. This is surprising as the formation of a bulk compound can safely be excluded. Oxygen must have induced re-crystallisation at a temperature of 87% of the melting point. The still sharp diffraction lines exclude a possible cracking-re-orientation as mechanism of re-structuring and require the assumption of extensive internal mass transport as re-orientation of grains larger than 80 nm in diameter is not a very likely procedure. These observations are well in line with the fact that silver foils become good oxygen separation membranes in the temperature range in question and that they can effectively separate oxygen from nitrogen which has no permeability through silver.

Fig. 4 presents the geometry of the (331) surface and reveals that this face is an open variety of the (111) face of a close-packed structure. The fact that this high-indexed termination dominates the external surfaces of the silver crystallites indicates that oxygen exerts a stabilizing influence on this geometry. It is noted that in several earlier studies (see references for Table 1) the special effect of defects on the activity of a silver surface for oxygen adsorption was mentioned. The (331) surface can be considered as a defective surface by default.

The extensive mass transport associated with the re-crystallization of the foils is indicated by morphological studies. Fig. 5 reveals for sample 2 by AFM inspection that the initially present weakly corrugated hill-and valley surface of the foil is drastically re-structured and is densely faceted with a saw-tooth profile. The steep slops of the facets (Fig. 5C) exhibit a step-and-terrace structure with varying step heights allowing the development of bent contours of the facets. The symmetric shape of the highly oriented

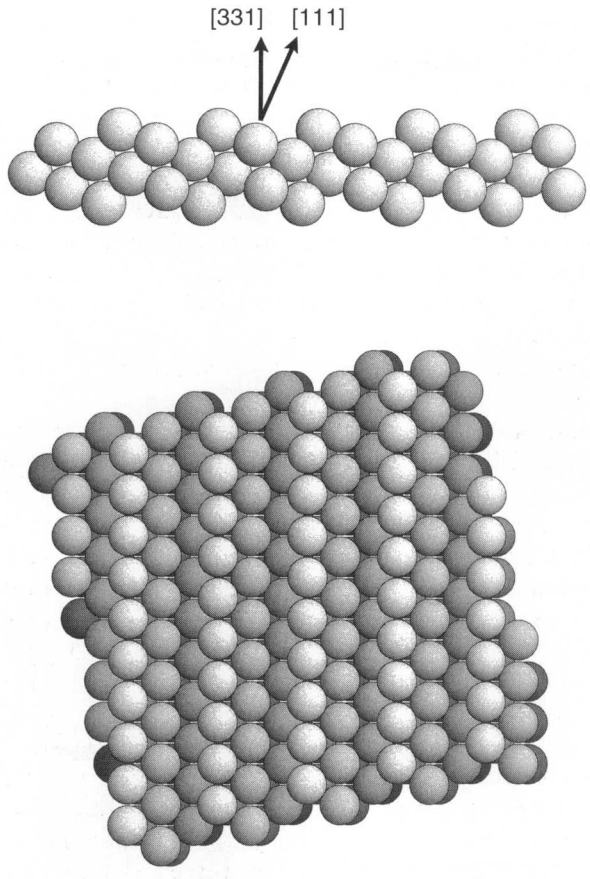

Fig. 4. Schematic views of the Ag (331) surface. This orientation contains terraces of (111) orientation. The angle between the two planes occurs in the rocking curve of Fig. 7a.

facets and the dense coverage of the whole foil surface which are the impressions of the AFM images 5A and 5B are reflected in the X-ray diffraction profile of this specimen (a reproduction experiment to that of Fig. 3c). Investigations in the temporal evolution of this re-structuring reveal that with increasing annealing time the features do not grow in size but the coverage of the initially flat surface increases with time.

Fig. 6 reveals in SEM images the extent of mass transport during treatment in pure oxygen (sample 3). The change in surface morphology between the samples (1 and 3) is apparent. The lower image shows a rare situation where the facetting has not covered the whole surface. A grain boundary between two large crystallites denotes the border line of the facet-

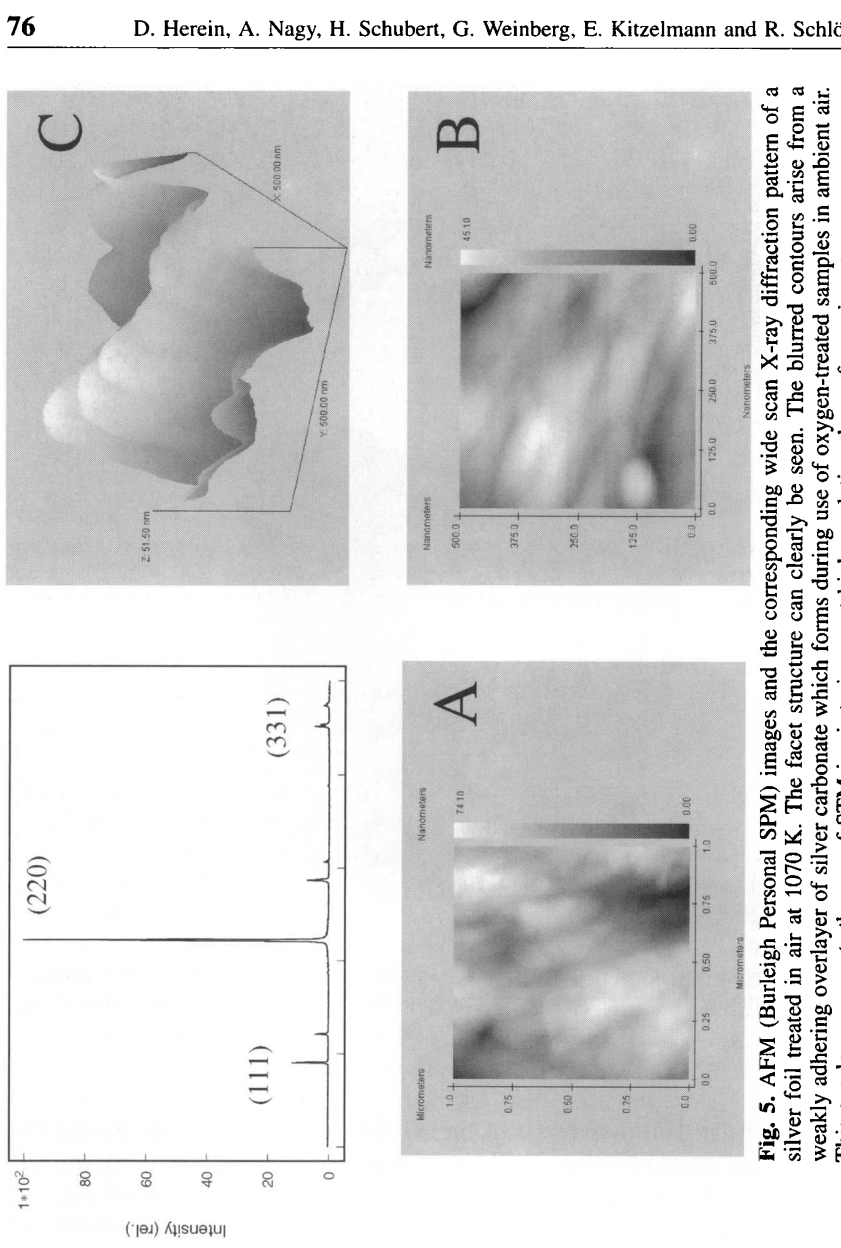

Fig. 5. AFM (Burleigh Personal SPM) images and the corresponding wide scan X-ray diffraction pattern of a silver foil treated in air at 1070 K. The facet structure can clearly be seen. The blurred contours arise from a weakly adhering overlayer of silver carbonate which forms during use of oxygen-treated samples in ambient air. This overlayer prevents the use of STM in air to image at high resolution the surface microstructure.

ting. This reveals the structure-sensitivity of the process. The surface orientation of the neighbouring grains is apparently different with the right hand grain being more susceptible to re-structuring than the left-hand grain. The smooth appearance of the terraces in Fig. 6B is an instrumental artefact.

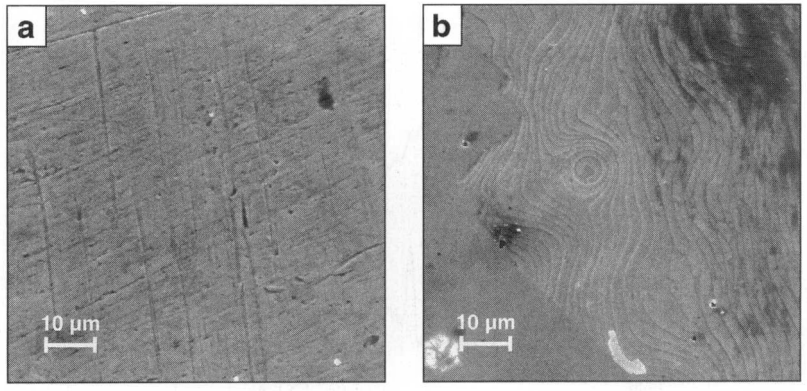

Fig. 6. SEM (Hitachi S 400, 15 keV) images of samples 1 (a) and 3 (b). The white particles are remains from polishing materials (a) and silver silicates (b). The stripes in (a) are polishing marks of the commercial sample. The dark contrasts arise from beam damaging experiments of the silver carbonate overlayer creating an insulating film giving rise to high secondary emission at moderate acceleration voltages (not present at 30 keV).

STM images of such surfaces [9] revealed that they are fully faceted with a similar saw-tooth arrangement as depicted in Fig. 5 but with a different orientation.

The technique of rocking curves is well-suited to determine the average orientations of the crystallites in a foil sample. A fully random orientation of the crystallites leads to smooth intensity distributions containing a constant angle-independent contribution from the crystallites and an angle-dependent component from various geometric influences on the diffracted intensity caused by sample perfection and by the experimental set-up. Such a situation is seen in the rocking curve of the (111) reflection for sample 1 shown in Fig. 7c. The sharp spike at around 20 deg Ω indicates a preferred orientation of some crystallites in the untreated sample which was already deduced from the integral intensity distribution of Fig. 3. Oxidation in air causes the silver foil to become strongly preferentially oriented as already seen in the previous experiments. The degree of relative orientation of the facet wedges is, however poor as follows from the complex multi-peak structure of the rocking curve in Fig. 7b. The fine structure of the peaks contains information about the bending of the facets as seen in the AFM data and about the step heights at their slopes. The increase of the oxygen partial pressure from that in air to pure oxygen causes further re-structuring with almost perfect relative orientation of the facets and exclusive parallel orientations. This follows from the peak structure of the corresponding rocking curve in Fig. 7a. The angular distance of the main peaks reflects the angle between the (111) and (331) planes as shown in Fig. 4. A slight discrepancy with the theoretical distance and the satellite lines are caused

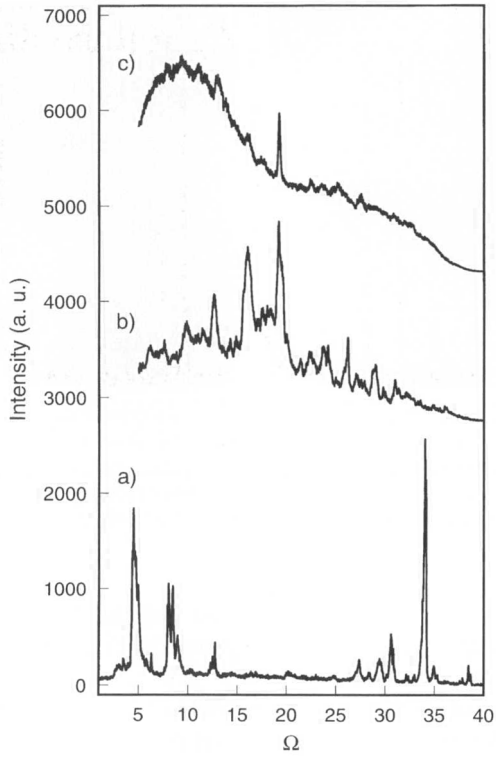

Fig. 7. Omega scans (rocking curves) around the (111)-reflection of silver for (c) untreated Ag-foil (Sample 1), (b) oxidized Ag-foil in 20% oxygen (Sample 2) and (a) oxidized Ag-foil in 100% oxygen.

again by the imperfection of the diffraction geometry due to the non-perfectly flat sample surface. The very narrow line profile indicates the perfection of the relative orientation of all facets. The fact that no intensity is seen in-between the peaks confirms the complete re-structuring of all silver within the diffracting volume and manifests the pronounced effect of the oxygen treatment on all silver atoms in the sample without the possibility of forming a binary compound.

The detailed analysis of the diffraction pattern from Fig. 3c with respect to intensity and position reveals several differences to the pattern of Fig. 3a and 3b. These differences are related to the presence of oxygen in the average bulk volume of the sample. A pure surface effect of the oxidative treatment which would be undetectable in the present type of X-ray diffraction experiment. The top profile in Fig. 8 reveals that static disorder (no qualitative change at high measurement temperatures) exists in the silver after oxygen treatment. The broad structures under some peaks indicate the presence

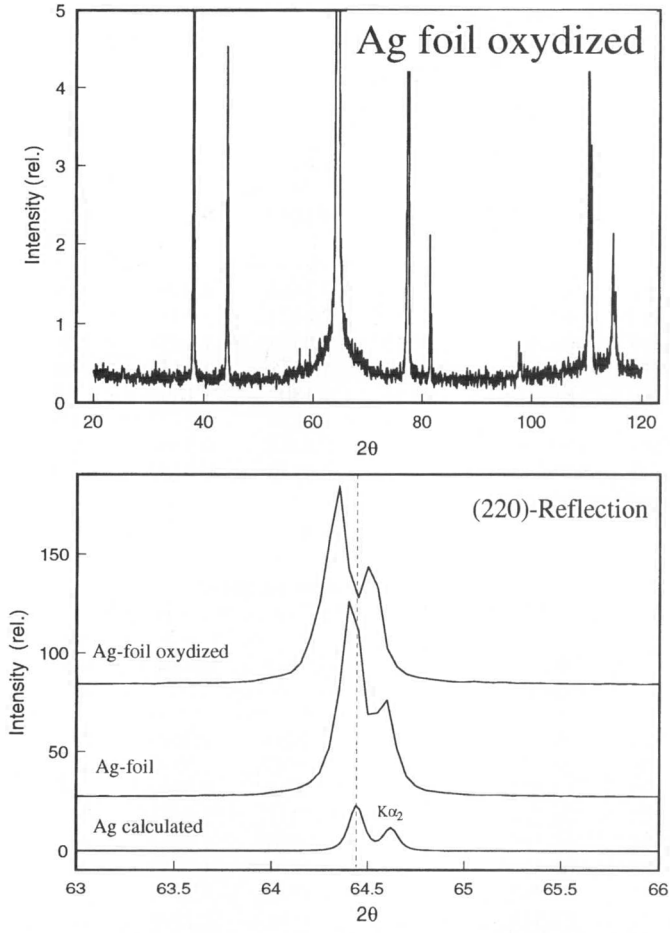

Fig. 8. High resolution XRD of sample 2. The top panel shows the weak additional intensities under some Bragg reflections ("foot" profiles). The lower trace shows for the (220) reflection the deviation in position and intensity compared to the calculated peak from the fcc cubic silver structure.

of broad additional diffraction lines which can either be due to superlattice reflections or they indicate a lowering of the cubic symmetry of the silver after oxidation. An interpretation as disorder peaks of cubic silver is excluded, as the foots do not occur under all Bragg peaks of the cubic phase. A possible unidirectional incorporation of oxygen as reason for the additional diffracted intensity is in line with the very pronounced parallel orientation of the facets (see Fig. 5) and with the operation of silver foils as gas separator membranes for which diffusion channels are required. The lower panel

Table 2. X-ray diffraction data of samples 1 and 3. The positions and intensities result from least square fits of all experimental lines shown in Fig. 3. a(theo) refers to JCPDS 4-0783.

Sample 1

	a(obs.) = 4.0892(5) Å			a(theo.) = 4.0862 Å			
No.	2Θ (obs.)	2Θ (calc.)	obs.-calc.	d(obs.)	d(calc.)	Int. (rel.)	*hkl*
1	38.161	38.085	0.0759	2.3564	2.3609	29.9	111
2	44.322	44.264	0.0571	2.0421	2.0446	23.5	200
3	64.409	64.389	0.0193	1.4454	1.4458	100	220
4	77.326	77.329	−0.0032	1.2330	1.2329	19.8	311
5	81.487	81.467	0.0194	1.1802	1.1805	4.3	222
6	97.765	97.787	−0.0227	1.0225	1.0223	1.9	400
7	110.383	110.390	−0.0071	0.9382	0.9381	10.7	331
8	114.770	114.795	−0.0252	0.9145	0.9144	7.3	420

Sample 3

Orthorhombic solution a-centred:
a = 4.092(2) Å; b = 2.896(2) (Å; c = 2.886(1) Å

No.	2Θ (obs.)	2Θ (calc.)	obs.-calc.	d(obs.)	d(calc.)	Int. (rel.)	*hkl*
1	37.968	38.027	−0.0597	2.3680	2.3644	1.4	110
2	38.140	38.122	0.0181	2.3576	2.3587	1.0	101
3	44.243	44.229	0.0136	2.0456	2.0462	3.5	200
4	44.321	44.264	0.0574	2.0421	2.0446	0.5	011
5	64.340	64.361	−0.0218	1.4468	1.4463	19.9	211
6	64.508	64.518	−0.0096	1.4434	1.4432	2.4	002
7	77.238	77.242	−0.0040	1.2342	1.2341	2.0	310
8	77.373	77.411	−0.0384	1.2324	1.2318	0.8	112
9	110.432	110.422	0.0094	0.9379	0.9379	100	312
10	110.489	–	–	0.9376	–	2.9	
	114.782	114.765	0.0164	0.9144	0.9145	3.4	222

of Fig. 8 presents a high resolution scan through the (220) reflection. The lower plot shows the position and intensity expected for a statistical sample. The cold working of the foil production led to a significant increase of the intensity with very little variation of line profile and line position. The crystallites in the silver were re-oriented during manufacture. The intensity of the (220) reflection is further increased after oxidation, the profile has changed (see top panel) and so has the position. The shift of 0.08 deg to lower diffraction angles indicates an increase in the lattice spacing. This shift occurs not simultaneously with all diffracted lines excluding a

measurement error or a simple expansion of the cubic lattice due to either incorporated oxygen atoms or as consequence of an isotropically enhanced defect density. Table 2 reports the fitted line positions for samples 1 and 3 according to precision profile analysis and after X-ray satellite correction. The data of sample 1 exhibit only for the first two reflections discernible deviations from the expected positions. These deviations are due to an apparent misalignment of the sample caused by its rough surface. The very small increase of the lattice spacing relative to the literature value a(theo) is ascribed to the presence of defects which reduce the average sample density and to the limited accuracy of the alignment of the present sample and the reference in the literature (see Table 2).

It is not possible to maintain the cubic lattice symmetry of the oxidized silver with fitting all of the observed intensities and to minimize the positional deviations. The highest symmetry which fits the data and which exhibits the best ratio between observed and observable reflections (20/10) is a centred orthorhombic cell. The a-centred model used in Table 2 is one possible model which cannot be discriminated with the present data from other centred structures. This fit explains all foot structures such as shown in the lower panel of Fig. 8. It explains well the varying degree of deviation in position from the expected value for cubic silver for different Bragg peaks. The model also accounts for the intensity distribution which is not only due to texture (as discussed above) but which can also be accounted for by a lowered symmetry of the unit cell. The significant deviation of the unit cell parameters are due to symmetry effects and are not the consequence of strongly changed positions of the silver atoms in the unit cell. The positional deviations are barely visible in the atom co-ordinates. The action of the oxygen atoms has caused a slight gliding of layers of silver atoms out of their close-packed arrangement. This gliding causes the formation of a lattice anisotropy along a high-indexed direction which we assign to the preferential direction along which oxygen diffuses through the metal lattice. The same slightly distorted lattice also explains well the intensity distribution of the diffraction pattern of Fig. 3.

Temperature programmed desorption

The X-ray diffraction data show clearly that the interaction of oxygen with silver has drastic effects on the bulk structure of the metal without any indication for the formation of a binary compound. Chemisorption of oxygen atoms should thus reveal complementary information about the surface structural changes. The bulk of the experimental data mentioned in Table 1 allows the use of oxygen TDS data as chemical probe for the activity of the sample to chemisorb the three species identified in earlier work.

Fig. 9 presents TDS traces of a high-pressure isobaric exposure series on sample 4. The results are in agreement at first glance with the surface

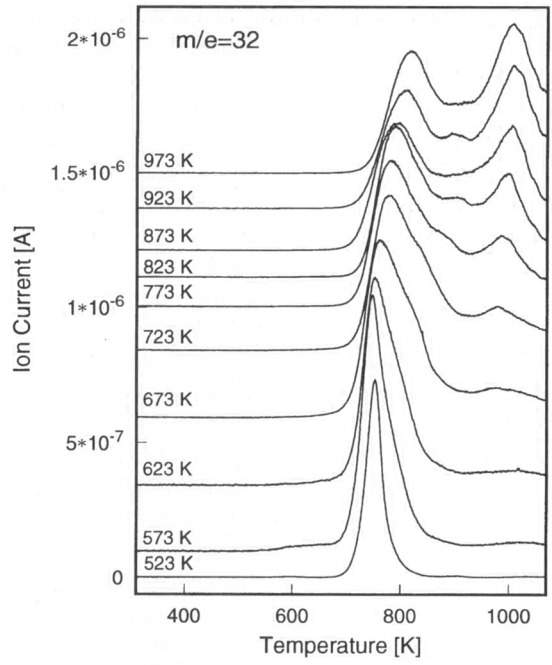

Fig. 9. Oxygen TDS data for sample 4. Exposure conditions were 10 mbar oxygen for 5 min at the temperature indicated in the Fig.. The sample was always cooled in oxygen atmosphere.

science studies on single crystals revealing a single peak of atomic adsorbed oxygen at low exposure temperatures. Lower exposure temperatures than 525 K are not possible due to the unwanted interference with the formation of a silver carbonate species with hdrocarbon impurities of the oxygen serving as carbon source [4, 13]. With increasing exposure temperature we observe the formation of the assigned γ species at 623 K and the growth of a diffuse structure in-between the initial peak and the γ species. In addition, the initial symmetric peak seems to shift to higher temperatures. The assignment in the literature was that the diffuse species arises from bulk-dissolved oxygen (β species).

The pre-treatment of the silver grains with oxygen (sample 5) was intended to saturate the bulk of the sample and so possibly to enhance the resolution of the TDS experiment. In addition, all possible organic contaminants should be removed which minimizes the interference of their oxidation with TDS experiments. Fig. 10 shows the results. At low exposure temperatures this strategy was indeed successful revealing a split first peak into a saturated (from pressure-dependent experiments) low-temperature signal and a sharp second signal which started to broaden drastically with

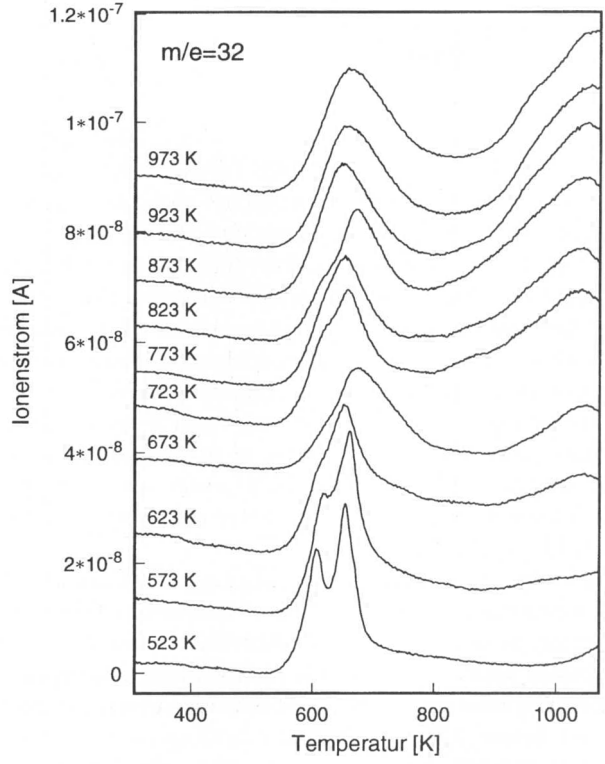

Fig. 10. Oxygen TDS data for sample 5. The experimental procedure was exactly the same as for the data of Fig. 9.

increasing exposure temperature. This diffuse signal is assigned to the bulk-dissolved species. At 623 K exposure temperature the γ state starts to become populated as in the previous series. Its true position and intensity is difficult to locate due to the massive overlap with the diffuse peak from bulk-dissolved oxygen. The experiment shows that above 573 K the bulk-dissolved species becomes activated and starts to exchange with surface oxygen species. It is noted that the position of the low-temperature peak in Fig. 10 is in good agreement with the data from single crystal studies [13].

In order to check the assignment of the peaks a quantification of the desorption signals was carried out. The ratio of oxygen to silver surface atoms (assumed to be $1 * 10^{15} * cm^{-2}$) is 1.1 to 1.9 for the double peak feature in Fig. 10 which is in good agreement with the assignment given. At higher exposure temperatures the resolution into individual peaks is no longer possible and only the integral desorption signal can be used to illustrate that the TDS peaks have very little to do with surface chemisorbed

species and support clearly the notion [1] that under the chosen conditions the bulk of the sample interacts strongly with oxygen atoms. The quantification for Fig. 9 gave values for the oxygen-to-silver ratio of 6.6 at 523 K, 16.6 at 723 K and 20.0 at 923 K.

The idea that with increasing desorption temperature the oxygen is coming from deeper layers of the sample was further supported by the observation that at 0.10 K/s heating rate the complex spectrum collapsed into two sharp lines at 570 K and at 900 K increasing the heating rate revealed a strong shift of the low-temperature peak with faster rates to higher temperatures as expected for a high order desorption process. The high temperature peak became split into a weak signal independent of the heating rate and developed satellites with a weaker dependence of position on the heating rate as the low-temperature peak. This complex behaviour is due to a continuous change of the rate-determining step from a surface process for the low-temperature peak over a distribution of diffusion-controlled processes characteristic for the depletion of the bulk reservoirs to an apparent first-order process of bond-breaking between silver and oxygen characteristic for the strongly held γ species.

The complexity of the TDS spectra displayed in Figs. 9 and 10 is also the result of a continuous transformation of the surface during heating as it is to be expected from the structural observations. For this reason, all desorption processes above 775 K which marks a critical temperature for the kinetics of the structural transformations become strongly over-exaggerated at heating rates below 0.25 K/s. At faster heating rates the process occurs in interrupted stages and the same effect is thus observed as a function of the number of repetitions of the TDS experiment. We followed the evolution for sample 4 up to 79 successive experiments with the result that the first sharp peak in Fig. 8 almost disappeared and the γ peak became a single dominating feature peaking at 925 K.

Sample 1 proved to be much more resistant to these structural transformations interfering with the desorption processes than the silver granules. For this reason it was possible to follow at fixed exposure temperature the effects of increasing exposure pressure and the modifications of the restructuring on the desorption features.

In Fig. 11 the evolution of the $\alpha + \beta$ desorption peak with increasing oxygen pressure is followed. Raising the pressure over 4 order of magnitude caused about a threefold increase in chemisorbed oxygen with a very strong decrease of the effect with increasing pressure. This is regarded as a characteristic feature of a sub-surface deposition of oxygen in which the barrier of the diffusion into the bulk is "compensated" by the increase in chemical potential of the solute in the gas phase. The surface species is of course present at all exposure pressures and already fully saturated at the lowest pressure applied. The small difference between the difference peaks in Fig. 11 at low temperatures is the signature of the α species. This difference

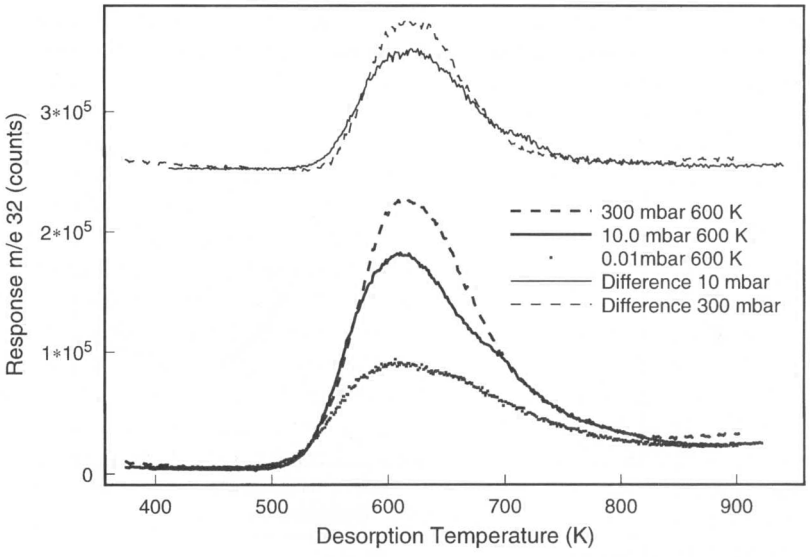

Fig. 11. Evolution of the low-temperature TDS feature from sample 1 after pre-oxidation seen in Fig. 13 with increasing exposure pressure at fixed pre-oxidation temperature. The exposure temperature was 575 K, the exposure time was 5 min. The shoulder at about 700 K in the 10 mbar spectrum arises from an interference of a silver film deposited on the inner wall of the reactor. The small signal from this material requires no temperature correction and is thus displaced. No normalization of the ordinates was necessary for the difference signals shown in the upper part of the Figure.

remains independent of the exposure pressure as was checked by series of difference spectra. The position of the feature remains fixed for all exposure pressures at 545 K which is again in good agreement with low-pressure single crystal data.

The *in situ* X-ray diffraction experiments revealed that in pure oxygen the re-structuring from (110) texture to (311) texture becomes facile at about 800 K which is in good agreement with the onset of TDS modifications at 775 K described above. The effect of this re-structuring on the TDS spectra was studied with the preparation of samples 2 and 3 from the same foil which was used for sample 1. The effects are summarized for two exposure pressures in Fig. 12. It occurs that the re-structuring has drastic effects on the desorption features. At 600 K pre-oxidation temperature, below the critical temperature, the dominating $\alpha + \beta$ peak is obtained at both exposure pressures. The composition of this peak by at least one broad and one narrow smaller component can be seen and compares to the situation displaced in Fig. 10 for the pre-loaded silver particles.

Above the re-structuring temperature, an intermediate desorption profile is seen for the 800 K sample. The γ and bulk-dissolved species formed after

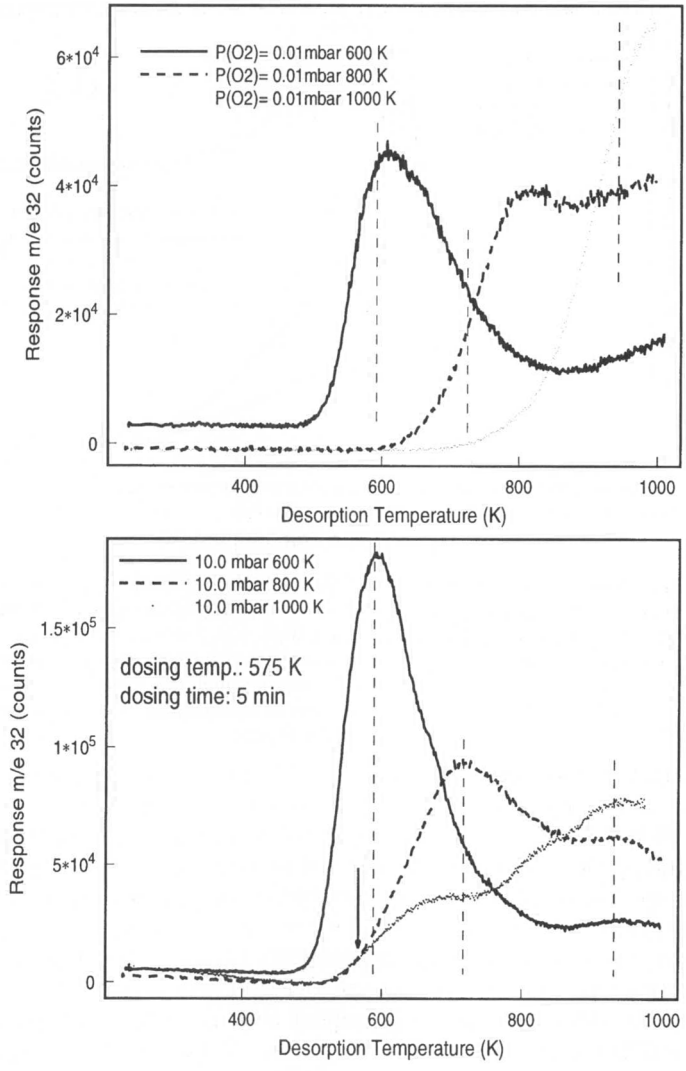

Fig. 12. Oxygen TDS results from sample 1 after pre-oxidation in flowing oxygen at the temperatures indicated. At fixed dosing times and temperatures the exposure pressure was varied. The dashed lines are guides to the eye. The solid arrow in the lower panel marks the exposure temperature.

the 1000 K pre-treatment. The abundance of these species depends critically on the oxygen partial pressure. At 10^{-2} mbar which is far above the usual UHV exposure pressures, only the bulk-dissolved β species was observed. The 1000 K pre-treatment which transformed the foil into a fully faceted

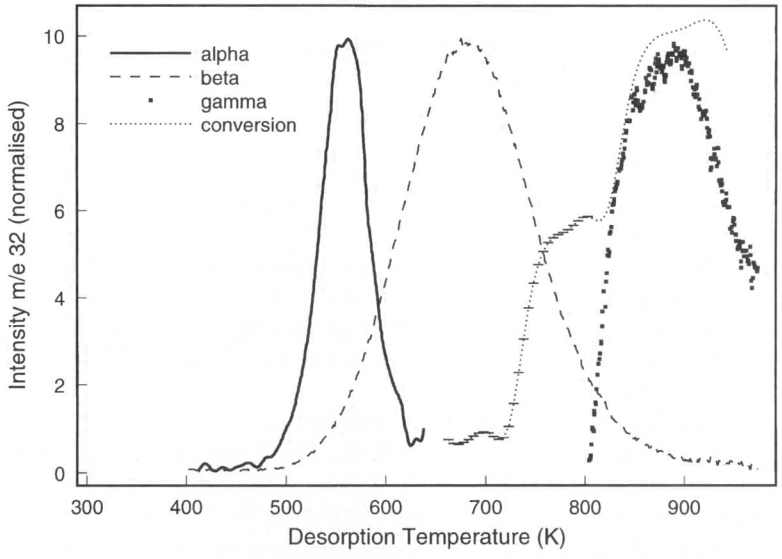

Fig. 13. Normalized desorption traces of the three individual atomic oxygen species on silver. The traces were obtained by successive difference formation between TDS data as shown in Fig. 12. The dotted line shows for comparison the conversion plot used in Fig. 1. For absolute values of conversion see the second ordinate in Fig. 1.

patchy single crystal surface (see Figs. 3, 4) inhibited oxygen chemisorption into states desorbing below 800 K. The high temperature feature in Fig. 12 (top panel) indicates the diffusion-limited segregation of dissolved oxygen atoms residing deep in the bulk. The heating rate of 1 K/s is too fast to allow the species to evolve at their surface desorption temperatures.

The situation is completely different at 10 mbar exposure pressure as can be seen from the lower panel in Fig. 12. The dominating feature is now the bulk-dissolved species with two features below 800 K and a small γ peak at 890 K. This small feature is saturated when raising the pressure to 300 mbar which causes the bulk-dissolved feature to grow by over an order of magnitude in intensity. The strong pressure-dependence of the oxygen dissolution was not observed with untreated sample 1, allowing to conclude that the pre-oxidation of the silver increased the reactivity towards dissolution of oxygen significantly. The finding of a slight bulk lattice distortion in the X-ray analysis fits well to this effect.

The good reproducibility of the desorption profiles from the oxygen pretreated foil samples and the marked pressure dependence of the population of the strongly held γ species allowed separation of the desorption profiles into the individual contributions from the three respective features. The complex line profile and the apparently variable desorption temperatures of

the different species in Figs. 8 and 9 are physically inconsistent and are viewed as the result of a variable superposition of the three species with the additional complication of a great variability of the abundance of the bulk-dissolved species. The β species is expected to exhibit the widest peak profile due to the interference of diffusion processes from varying depth with the desorption kinetics. The analytical discrimination of the three basic desorption features from the TDS data set of samples 1 to 3 is reported in Fig. 13.

The α species desorbs in a narrow symmetric feature at 565 K and is saturated at all pressures applied in this study. Its intensity is, however in the range of a few % of the total desorption feature and thus not well recognized in the raw data. The peak is in fair agreement with the leading peak at low temperatures in Fig. 10.

The β species desorbs for all bulk-saturated samples at the present TDS conditions in a symmetric feature at 680 K. The linewidth is large relative to that of the α species and the profile becomes skewed to higher temperatures with increasing undersaturation of the silver bulk, as then desorption and dissolution in the bulk compete and complicate the desorption kinetics. Examples of such skewed line profiles can be seen in Figs. 8 and 9 for exposure temperatures of above 700 K. The intensity of the β desorption peak for sample 3 and for an exposure pressure of 300 mbar was found to be 32 times that of the α peak which is in fair agreement with the integration results from the spectra of Fig. 8. The threshold pressure of the formation of β oxygen depends on the surface perfection and is as low as 0.05 mbar for sample 1 and as high as 10 mbar for sample 3.

The desorption feature of the γ species occurs as a small structure at the high-temperature side of the large β peak. It was not possible to recover the undisturbed peak profile due to the interference with the delayed desorption from deep zones of the silver bulk. Its intensity is of the same order as that of the α species. The peak at 880 K is saturated only at 100 mbar exposure pressure and exhibits a threshold pressure of 5 mbar below which the γ species does not form.

Discussion

A combined analysis of the effects of oxidation of elemental silver at high temperatures and oxygen pressures between 0.01 and 300 mbar with structural, morphological and thermal desorption methods revealed that the metal is not inert in oxygen despite the thermodynamic instability of the most stable oxide phase.

X-ray diffraction excluded the occurrence of a crystalline oxide phase. Analysis of the integrated intensity distribution and rocking curve experiments illustrated, however, that the bulk of the sample is re-structured after

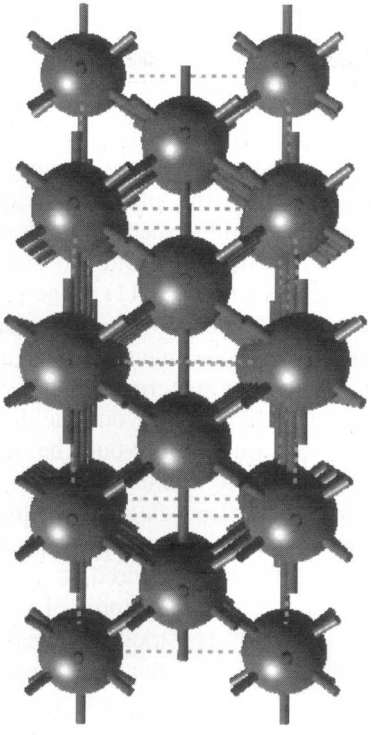

Fig. 14. Ball and stick model of silver in a projection close to (220). No relative height of the atoms can be seen. The projection indicates the "channel" structure in exaggerated way as the silver structure is close-packed. The kinetic diameter of the oxygen atoms is difficult to asess without knowing its electronic charge.

the exposure to high temperature and oxygen. The preferential orientation of the crystallites terminates at the surface with pronounced faceting. The orientation of the facets changes as a function of the oxygen partial pressure applied from (110) to (331). The peak profile analysis of high resolution scans revealed positional variations and the occurrence of extra diffraction lines close to the parent cubic silver Bragg peaks. These extra features can be accounted for with a slight deviation of the silver atom positions from their close-packed positions giving rise to a symmetry reduction from cubic to centred orthorhombic. A slight anisotropy of the silver atom arrangement which finds its parallel in the surface morphology of perfectly aligned trigonal facets is seen as the consequence of the penetration of oxygen atoms into the silver lattice along "channels" which are oriented along high-indexed crystallographic directions. These directions exhibit low atom densities and are thus energetically favourable for a slight reduction in the metal bonding which is required to create sufficient space for efficient transport

of the oxygen in the lattice. The critical temperature for this bulk structural transformation is at about 700 K. Below this limit the process occurs so slow that it remains undetected on the present time scale of about 24 h.

The structural effects are visualized in Fig. 14. It shows a projection of the silver lattice down to the (110) face. This face exhibits parallel "channels" arising from coupled voids of the close packing. In order to allow the penetration of an additional atom, the silver atoms of the central layer in Fig. 14 have to move slightly with respect to each other. This requires a slight distortion of the other atoms to avoid too close contacts. It can be seen that the atom displacement in the (111) plane (diagonal in Fig. 14) is very much less than the displacement in the projection plane which is in agreement with the irregular displacements of the apparent cubic lattice constant in the X-ray diffraction pattern. Such a complicated atom rearrangement may be energetically more favourable than the isotropic swelling of the close-packed structure which would be an alternative mode of adapting the channel widths to the kinetic diameter of the oxygen atoms. These atoms cannot carry a significant negative charge as they would then not fit through the channels. The critical temperature may indicate a certain dynamic disorder by thermal motion required as an additional measure to facilitate the penetration of the oxygen atoms. The finding of a slightly distorted bulk silver structure is in remarkable agreement with results from surface science experiments and their theoretical analysis [13, 19] which predict an optimum fit between oxygen and silver at the (110) surface after introduction of slight distortions in such a way that the oxygen adatoms sit over the terminations of the "channels" shown in Fig. 14.

Thermal desorption spectroscopy proved to be sensitive to the surface structural alterations as well as to the propensity of the material to accept bulk-dissolved oxygen. The silver granules seemed to be much more reactive to oxygen-induced re-structuring than silver foil, an observation which is in agreement with a literature report about silver powder [14]. The different density and disposition of lattice defects in these two materials is seen as the cause for this purely solid-state kinetic effect.

Quantification of the TDS profiles revealed that the features are dominated by sub-surface processes, as the desorbed amount of oxygen greatly exceeded the number of possible surface sites, even more than was reported in the literature (1).

The oxidative pre-treatment of the silver foils led to saturation of the metal bulk with oxygen and thus blocked the reaction channel of thermally induced bulk dissolution of sorbed species [13]. This procedure, which simulates an activated catalyst material, allows enhanced resolution and reproducibility of the TDS experiments to an extent that pressure dependencies and the isolation of three fundamental desorption features becomes possible. The resulting features are in full agreement with the previous assignment [4, 8, 9] given in Table 1. The data of Fig. 13 are further in

agreement with all other observations reported in Table 1, if one considers the complicating effect of unrecognized superposition of the bulk-dissolved species over the desorption features from the surface species. The superposition effect also accounts for the significant uncertainties in the reported desorption temperature maxima.

An inhibition effect of the surface re-structuring on the formation of the γ species was clearly observed. This effect which was also described in a study with silver powder [14] is tentatively explained by the initial formation and saturation of the (331) re-crystallized surface with the γ state during oxidative pre-treatment. The high stability of the γ phase prevents its decomposition at exposure temperatures of 565 K and inhibits thus the adsorption of more oxygen on or below the re-structured surface. This would imply that no surface atomic oxygen can be adsorbed on top of the γ phase. Only at 10 mbar exposure pressure is the reaction channel for the formation of β oxygen opened again allowing further oxygen uptake of the fully (331) re-structured sample below the surface. The mobility of adsorbed oxygen atoms into the bulk of silver upon further oxygen exposure was already described much earlier in the literature [20] in a study with Ag(111).

This inhibition can also be understood on the basis of the structural data. The (331) face does not exhibit channels between atoms so that the structure shown in Fig. 14 is lost at the surface of the crystallites. Only there can the γ species exist as monolayer [8, 10] reducing the surface energy of the silver in pure oxygen [15] below the value of the (110) oriented distorted silver phase prevailing at lower partial pressures of oxygen. The surface re-structuring requires for its registry [16] with the underlying atoms a re-structuring of the bulk. This is achieved within the information depth of the X-ray diffraction experiment of several microns by growing facets as seen in Fig. 6. These facets make up for most of the diffracting volume and cause the drastic change in intensity distribution seen in Fig. 3. The present experiments cannot answer the question about the complete bulk re-structuring below the information depth. From the documented fact of the macroscopic shape transformation in practical catalysts [3, 7, 15] it is assumed that upon sufficient oxygen exposure time the whole bulk will re-structure from the (110) orientation into the (111) orientation.

The analysis of the present results in terms of their relevance for the practical catalytic action of silver is complicated by the fact that reaction gas atmospheres are mixtures of oxygen, inert gases and reducing organic substrate molecules. A typical situation of co-adsorption effects has to be expected precluding quantitative extrapolations of the present results (i.e. threshold pressures) to the catalytic situation. The fact that in previous TPRS and instationary high pressure reaction experiments [9] complete internal consistency was reached allows to conclude that the overall adsorption characteristic of silver in reaction atmospheres containing molecular oxygen will be dominated by the silver-oxygen interaction. The relevance

of the present qualitative findings for the catalytic application of silver in the selective oxidation of methanol to formaldehyde can be seen from Fig. 13. In a previous study the parameter space of this reaction [8] was mapped out. In the temperature-composition section it was found that for most parameter settings one maximum occurs in the methanol conversion which corresponds for all compositions overstoichiometric in methanol to a maximum in formaldehyde formation. Only for a narrow range of compositions in which the oxygen abundance in the feed was close to the limit of stoichiometry, a second maximum of selective conversion was seen. This narrow range of parameters contains also the technical point of operation of the process [3, 8, 9]. The notion that essentially one reaction mechanism of oxydehydrogenation of methanol [2] should represent the main route to the selective conversion is not in line with the fact that the optimum of conversion and selectivity is in a composition range still understoichiometric in oxygen. In addition, a significant amount of molecular hydrogen is produced in technical reactions pointing to the operation of a dehydrogenation mechanism with formaldehyde and hydrogen as products. This combined operation of two mechanisms [7] requires two different surface sites as active centres [9] the existence of which was shown in instationary conversion experiments [8]. A section through the temperature-composition plane of the parameter space at a stoichiometry factor of 125:100 methanol to oxygen is inserted in Fig. 13. It is evident that the reaction occurs in a range of desorption processes resulting from the conversion of bulk-dissolved oxygen into surface oxygen. The α species formed from direct adsorption from the gase phase is not available to this reaction. Furthermore, the second maximum in conversion is exactly at the point, where the γ species becomes active in thermal desorption. It may be concluded that the second maximum in methanol conversion is due to the beneficial effect of the dehydrogenating γ species. The bulk dissolved species is of prime importance as it represents a vehicle to maintain a surface coverage with atomic oxygen at reaction temperatures which are above the stability limit of surface adsorbed oxygen from the gas phase (desorbing at 565 K). This allows one to conclude that the high reaction temperature required for the process is limited by the energy needed to activate the C−H bonds in the methanol molecule and not by the activation of molecular oxygen.

The mode of operation of the reaction requires the efficient interchange of the different oxygen species at the catalyst surface. Their relation is summarized in Fig. 15. At the gas-solid interface the two species α and γ can co-exist. The γ species requires high threshold temperatures and high oxygen partial pressures for its formation. These requirements determine in practical reactions the stoichiometry of the gas feed and not the need to stoichiometrically convert the primary reaction product hydrogen into water. Such a conversion is thermodynamically favourable as it shifts the equilibrium of dehydrogenation to the desired product side.

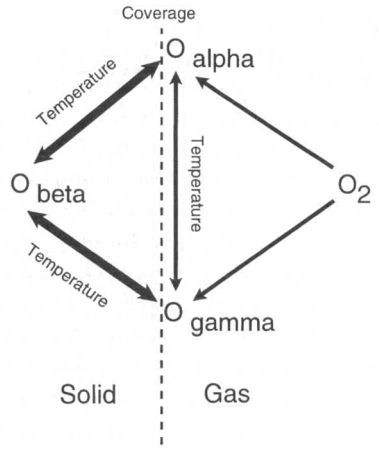

Fig. 15. Schematic representation of the relation between the three oxygen species and their modes of equilibration. At catalytic conditions for methanol oxidation the bulk-dissolved species plays an essential role in controlling the steady-state abundance of surface-adsorbed oxygen. During ethylene epoxidation both surface species can exchange without requiring essentially bulk-dissolved species.

At reaction temperatures for methanol conversion the α species does not exist in any large steady-state abundance at the silver surface. It occurs mainly as a transient species from the equilibrium exchange between bulk-dissolved and surface atomic oxygen, i.e. as consequence of the oxygen transport property of metallic silver at high temperatures. This property exists only in metallic silver at the given conditions, as the other reaction channel, to form an oxide from bulk-dissolved oxygen atoms, is thermodynamically closed. For this reason only silver and gold will be suitable as selective oxidation catalyst for this mode of operation. At the conditions of catalytic application all three species will be in efficient exchange with each other. For TDS analysis such an exchange is unfortunate as it tends to obscure the individual contributions from single desorbing species. The interchange mode is activated during the experiment and modifies the relative abundance of each species with progressive desorption. For model studies, at low coverage the equilibration may occur directly between the two surface species, provided the bulk reservoir is sufficiently empty. Otherwise, adsorption processes and segregation of previously stored oxygen will interfere with each other.

These complicating facts together with the interference of carbonate surface species and of restructuring lead to a complex sequence of events during the "simple" TDS experiments which explains the many conflicting reports in the literature [21] as indicated by the content of Table 1.

The TDS data of Fig. 13 allows one to speculate about the relation of the present findings to the ethylene epoxidation process which differs fundamentally from the methanol oxidation reaction in the way that a stoichiometric amount of oxygen atoms has to be transferred onto the ethylene molecule without dehydrogenating any of the C−H bonds. Any reaction intermediate after breaking the C−H bond would be very susceptible to total oxidation via bonding of an oxygen atom on a single carbon atom. The transfer of the oxygen atom to the unsaturated bond is most efficiently achieved by a weakly held atomic species such as the α species. It is no coincidence that the desorption spectrum of Fig. 13 covers well the reaction temperature interval typical for the ethylene oxidation process. The present results are thus in full agreement with a substantial body of literature which relate the ethylene epoxidation to the presence of a weakly held atomic oxygen species [2, 22].

Conclusions

The present work highlights some general phenomena which occur in the extrapolation of surface-science results into the regime of surface chemistry at elevated pressures and temperatures. The silver-oxygen system exhibits a qualitative pressure gap between 10^{-4} and 10 mbar in which the dominating oxygen interaction changes from surface adsorption to sub-surface fixation and bulk dissolution. These latter two processes exhibit threshold conditions in pressure and temperature which are incompatible with standard UHV techniques. Yet these processes will affect the surface structure and chemistry and even modify the bulk metal structure. All this occurs without the possibility of forming an intermediate compound, a process which limits the conditions of metal-oxygen adsorption studies in most other metallic systems well within the boundary conditions of UHV experiments.

The data in Fig. 13 show that the only "UHV available" α species is not directly involved in the catalytic methanol oxidation. A detailed study of the kinetic properties of this species which is by a priori assumption a logical candidate for a reaction-determining species would lead to incorrect quantitative results, as the consideration of the diffusion processes controlling the equilibration with bulk-dissolved oxygen would not be possible. The second reactive species of γ oxygen is fully inaccessible to standard UHV experiments.

The study of the chemical and structural properties of any adsorbate on silver would, on the other hand, be impossible without the background and tools of surface science. With all the present information at hand, we still need to study the elementary steps in the reaction [9] in the way defined by the "single crystal approach" in catalysis with the modification that we use a more complex model surface than it is provided by a clean single crystal.

The present study shows that the tools of surface science and bulk structural methods can be applied to surface chemical situations provided that the complications induced by the participation of the bulk of the sample in the analytical responses are fully taken into account.

The present results can finally be considered as a plea to escape the confrontation between surface science and surface chemistry by closing the "gaps" between the two disciplines whenever possible with experiments rather than with extrapolations which rely on the difficult-to-prove condition that no discontinuities occur in the material properties between UHV and "high pressure" conditions. The present study reveals an example where this assumption cannot be made.

Acknowledgements

This work was supported by the Bundesministerium für Bildung und Forschung (BMBF). We acknowledge the long-standing co-operation with the BASF AG (Drs. Marosi, Essig, Krösche, Gallei) in the analysis of the selective methanol oxidation reaction.

References

1. G. R. Meima, L. M. Knijf, A. J. van Dillen, J. W. Geus, J. E. Bongaarts, F. R. van Buren and K. Delcour, Catal. Today **1** (1987) 117–131.
2. M. A. Barteau and R. J. Madix, in *The Surface Reactivity of Silver: Oxidation Reactions* (Eds.: D. A. King, B. P. Woodruff), Elsevier, Amsterdam **1982**, vol./4, p. 95.
3. G. Reuss, W. Disteldorf, O. Grundler and A. Hilt, *Formaldehyde*, Verlag Chemie, Weinheim, **1988**, vol. A11, p. 619.
4. C. Rehren, M. Muhler, X. Bao, R. Schlögl and G. Ertl, Z. Phys. Chem. **174** (1991) 11–52.
5. G. Rovida, F. Pratesi, M. Maglietta and E. Ferroni, Surf. Sci. **43** (1974) 230–256.
6. R. Haul, Z. Phys. Chem. **186** (1994) 227–230.
7. H. Sperber, Chemie-Ing.-Techn. **41**(17) (1969) 962–966.
8. H. Schubert, U. Tegtmeyer and R. Schlögl, Catal. Lett. **28** (1994) 383–395.
9. H. Schubert, U. Tegtmeyer, D. Herein, X. Bao, M. Muhler and R. Schlögl, Catal. Lett. **33** (1995) 305–319.
10. X. Bao, M. Muhler, B. Pettinger and R. Schlögl, G. Ertl, Catal. Lett. **22** (1993) 215–225.
11. V. I. Bukhtiyarov, A. I. Boronin and O. A. Baschenko, Surf. Ref. Lett. **1**(4) (1994) 577–579.
12. C. Rehren, G. Isaak, R. Schlögl and G. Ertl, Catal. Lett. **11** (1993) 253.
13. C. T. Campbell, Surf. Sci. **157** (1985) 43–60.
14. M. Bowker, P. Pudney and G. Roberts, J. Chem. Soc., Faraday Trans. I, **85**(8) (1989) 2635–2640.
15. X. Bao, G. Lehmpfuhl, G. Weinberg, R. Schlögl and G. Ertl, J. Chem. Soc. Faraday Trans. **88**(6) (1992) 865–872.
16. X. Bao, J. V. Barth, G. Lehmpfuhl, R. Schuster, Y. Uchida, R. Schlögl and G. Ertl, Surf. Sci. **284** (1993) 14–22.
17. G. E. Rhead and H. Mykura, Acta Metall. **10** (1962) 843.
18. K. C. Prince, G. Paolucci and A. M. Bradshaw, Surf. Sci. **175** (1986) 101–122.

19. T. Schimizu and M. Tsukada, Surf. Sci. Lett. **295** (1993) L1017–L1022.
20. G. Rovida, F. Pratesi, M. Maglietta and E. Ferroni, Surf. Sci. **43** (1974) 230–256.
21. J. S. Ozcomert, W. W. Pai, N. C. Bartelt and J. E. Reutt-Robey, Phys. Rev. Lett. **72** (1994) 258–261.
22. J. T. Gleaves, A. G. Sault, R. J. Madix and J. R. Ebner, J. Catal. **121** (1990) 202.
23. R. B. Grant and R. M. Lambert, Surf. Sci. **146** (1984) 256–268.
24. M. A. Barteau and R. J. Madix, Surf. Sci. **97** (1980) 101–110.
25. M. Bowker, M. A. Barteau and R. J. Madix, Surf. Sci. **92** (1980) 528–548.
26. X. Bao, J. Deng and S. Dong, Surf. Sci. **163** (1985) 444–456.
27. L. Lefferts, J. G. van Ommen and J. R. H. Ross, Appl. Catal. **31** (1987) 291–308.
28. V. I. Bukhtiyarov, I. P. Prosvirin and R. I. Kvon, Surf. Sci. **320** (1994) L47–L50.
29. V. I. Bukhtiyarov, A. I. Boronin, I. P. Prosvirin and V. I. Savchenko, J. Catal. **150** (1994) 268–273.